Critical issues in parameter calibration of cyclic models for steel members

Corrado Chisari [a,*], Antonella B. Francavilla [a], Massimo Latour [a], Vincenzo Piluso [a], Gianvittorio Rizzano [a], Claudio Amadio [b]

[a] University of Salerno, Department of Civil Engineering, University of Salerno, Via Giovanni Paolo II, 132, 84084 Fisciano (SA), Italy
[b] University of Trieste, Department of Engineering and Architecture, University of Trieste, Piazzale Europa, 1, 34128 Trieste, Italy

ARTICLE INFO

Accepted 14 November 2016

Keywords:
Hysteretic model
Pseudo-dynamic test
Strength degradation
Genetic Algorithms
Multi-objective optimisation

ABSTRACT

Accurate response predictions of steel structures subjected to earthquake loading involve the use of models able to simulate properly the cyclic behaviour of the regions where nonlinear phenomena take place. In case of full-strength joints, they are represented by the members connected, which may present softening response due to local buckling. Even though a number of phenomenological models have been developed in the last decades, their calibration seems to have received less attention. Usually, calibration is based on matching the experimental and numerical cyclic responses under loading protocols proposed by standards. Since these were not developed to this aim, the predictive capability of so calibrated models deserves investigation. In this work, a calibration procedure based on the minimisation of response misfit is presented and critically discussed, with reference to an experimental programme carried out at the University of Salerno. Different assumptions about the function to minimise, the ultimate rotation and number of objectives are compared and analysed. The main outcome of this investigation is that a calibration based on cyclic response only is not robust, since its accuracy under different loading conditions may deteriorate. The introduction of the monotonic test in a multi-objective framework may be effective, and its accuracy is confirmed by the results of pseudo-dynamic tests.

1. Introduction

Advanced seismic assessment of steel structures involves the use of numerical models able to represent nonlinear behaviour and account for damage in components. Although accurate predictions should in principle be obtained by using detailed finite element (FE) models in which the nonlinearities are included at material level [1,2], this approach results in an impractical computational effort, and thus simplified models based on concentrated plasticity are widely used in academic contexts [3–5] and, increasingly, in everyday professional practise. They are based on the concept that, if correctly designed, a structure manifests yielding in regions known a priori, which may be represented in the numerical model as ad-hoc zero- or finite-length elements, while the remaining parts of the structure can be modelled as elastic [6,7]. The accuracy of the simulation is thus driven by the behaviour of these elements, which should be able to represent, when applicable, hardening and softening, stiffness and strength degradation, pinching and gap closure, as in the case of full-strength connections [8], considered in this work, where the nonlinear behaviour is governed by local buckling of steel members. Widely used models with different degrees of sophistication were developed by Takeda [9], Bouc and Wen [10,11], Ramberg and Osgood [12], Richard and Abbott [13], Dowell et al. [14], Sivaselvan and Reinhorn [15], Ibarra et al. [16]. Being phenomenological rather than based on mechanics principles, all these models rely on some parameters that make them as general as possible to accommodate a number of different behaviours experimentally observed, but whose physical meaning is not immediately recognisable. An important phase prior to the seismic analysis is thus the calibration of the nonlinear elements modelling critical components.

Calibration is generally carried out by looking for the set of model parameters that, inserted in the model, fit the response measured in experimental tests as close as possible. The experimental data can be taken from purposely-performed tests [17], existing databases [18], or from results of numerical simulations by means of detailed FE models previously calibrated [19]. Often, the calibration tests are quasi-static cyclic tests following loading

* Corresponding author.
E-mail address: corrado.chisari@gmail.com (C. Chisari).

protocols proposed by the codes, e.g. the SPD protocol [20] for masonry, the ISO protocol [21] and the CUREE protocol [22] for timber elements, the EN 15129 [23] for anti-seismic devices, the ECCS protocol [24] and the AISC protocol [25] for steel structures. Loading protocols have been developed to give a reliable estimate of the cyclic deformation demand of the considered structural system. When dealing with structural elements characterised by nonlinear behaviour, demand strongly depends on the loading history and the hysteretic behaviour. For this reason, the formulation of the most advanced test protocols [22,25] is the result of a methodology involving: (i) selection of suitable set of earthquake ground motions; (ii) selection of representative structural models; (iii) calculation of cumulative seismic demands (by time-history analyses and statistical analyses of the results); (iv) construction of loading protocols meeting the evaluated cumulative seismic demands. It is evident that the results of such approach are influenced by the phases (i) and (ii), i.e. the protocol should be chosen according to the structural nonlinear behaviour of the element and the design earthquake characteristics. Regarding point (i), in [22] the authors used a non-degrading bilinear model, a peak-oriented (Clough) model and a pinching model accounting for stiffness and strength degradation; in [26] a specific protocol for short links in eccentrically braced frames was developed by modelling them as an ensemble of a standard beam element, multiple spring elements, and nodal constraints, as suggested in [27]; in [28] the authors utilised two variants of the Takeda model [9], the Wayne Stewart model [29] and a flag-shaped hysteretic model. AISC and CUREE protocols were developed considering records of natural earthquake ground-motions of Los Angeles with 10/50 hazard level (10% probability of exceedance in 50 years). In [22] the authors clearly pointed out that the demands obtained by applying this protocol are not representative of near-fault ground motions, distinguished by high-energy pulses, for which they propose another protocol; with the same arguments, a protocol for steel structures was developed [30], but neither was then adopted by standards. Mergos and Beyer [28] developed a protocol for European regions of low to moderate seismicity, after showing that the ordinary protocols impose higher cumulative damage demands. The variability of the cyclic performance of wood-frame shear walls depending on the loading histories is clearly underlined in [31].

Whereas loading protocols were developed with the aim of providing a reliable measure of the demand required to a structural sub-assemblage, they have now become a de facto standard even for the calibration of numerical hysteretic models, in particular for steel details [32,33]. However, this practice deserves some investigations. As pointed out above, a protocol is developed considering specific hysteretic models and earthquakes ground motions. It is not assured that a calibration based on that protocol is able to predict the response of the structural sub-assemblage even in case of different hypotheses, and some adjustments may be needed to achieve improved robustness. In this paper, the focus will be on the AISC protocol for ordinary ground motions, which represents the most used protocol for steel members, and the smooth model developed by Sivalselvan and Reinhorn [15], able to simulate a large number of phenomena encountered in cyclic response of steel members. A calibration procedure based on Genetic Algorithms (GA), already successfully applied to identification problems [34,35] is described and applied onto the results of a recently completed experimental programme. The applicability of the model obtained by calibration using different sources of experimental data is then assessed by validating the predictions against the outcomes of a pseudo-dynamic test.

2. Calibration of cyclic models for steel members

2.1. Overview

Calibration (or parameter identification) of a numerical model means finding the set of parameters $\tilde{\boldsymbol{p}}$ such that the computed response given by a simulation of a test $\boldsymbol{y_c}(\boldsymbol{p})$ is as close as possible to the experimental response $\boldsymbol{y_{exp}}$. This implies solving the optimisation problem:

$$\tilde{\boldsymbol{p}} = \arg\min_{\boldsymbol{p}} \omega(\boldsymbol{y}_{exp}, \boldsymbol{y_c}(\boldsymbol{p})) \tag{1}$$

where $\omega(\boldsymbol{y}_{exp}, \boldsymbol{y_c}(\boldsymbol{p})) = \omega(\boldsymbol{p})$ is a suitable cost function measuring the inconsistency between the experimental and computed quantities. One of the simplest and most widespread formulation for the cost function, adopted in this work, is:

$$\omega(\boldsymbol{p}) = \frac{1}{\omega_{\text{ref}}} \|\boldsymbol{y}_{exp} - \boldsymbol{y_c}(\boldsymbol{p})\| \tag{2}$$

where the operator $\|\cdot\|$ represents the Euclidean norm of a vector and $\omega_{\text{ref}} = \|\boldsymbol{y}_{exp}\|$ is a scaling factor needed to make ω non-dimensional. The minimisation of ω may be accomplished by using gradient-based methods (Trust region [36], Sequential Quadratic Programming [37]), or zero-order methods (Nelder–Mead algorithm [38], Genetic Algorithms [39]).

In the context of parameter identification, it is useful to remark the difference between *calibration* and *validation* test [40,41]. The former is the test introduced in formulation (1) to estimate the model parameters $\boldsymbol{p}$. The a posteriori comparison between the experimental results and the best model simulation serves as a preliminary assessment of the result. If the comparison fails, i.e. the two responses are found too different, this may be due to a problem either in the optimisation procedure (the real optimum has not been reached) or in the choice of the numerical model (the optimum has been attained, but the model cannot properly simulate the experimental response). If this check is positively passed, the calibration result has to be verified as regards its predictive capability. This is the objective of a *validation* test. The reasoning under this additional test is twofold. Firstly, it is very unlikely that, from a mathematical viewpoint, the relationship between parameters and response is bijective. Most often, the inverse problem of estimating parameters from the response is ill-posed, meaning that more than one solution corresponds to the same response fitting. When applied to a different loading condition, these multiple solutions may give responses significantly different from each other. Secondly, the mathematical model is always imperfect, and it may be accurate in predicting the response of a structure under some conditions, yet give poor approximation of the response in a different case. A test with different loading conditions is thus useful to investigate the applicability of the previously calibrated model.

The cost function defined in (2) is related to a single test. When N calibration tests are performed, the problem of how to collect information from different sources arises. The optimisation problem (1) becomes in this case:

$$\tilde{\boldsymbol{p}} = \arg\min_{\boldsymbol{p}} \{\omega_1(\boldsymbol{p}), \ldots, \omega_N(\boldsymbol{p})\} \tag{3}$$

where $\omega_i(\boldsymbol{p})$ represents the cost function value of the i-th test.

In the context of multi-objective optimisation, the concept of Pareto optimality replaces the usual notion of optimality [42]. In a minimisation problem, a solution $\boldsymbol{p_1}$ is said to dominate a solution $\boldsymbol{p_2}$ if and only if:

$$\begin{aligned} &\omega_i(\boldsymbol{p}_1) \leqslant \omega_i(\boldsymbol{p}_2) \quad \forall i = 1, \ldots, N \\ &\omega_i(\boldsymbol{p}_1) < \omega_i(\boldsymbol{p}_2) \quad \exists i = 1, \ldots, N \end{aligned} \tag{4}$$

A solution is referred to as Pareto optimal if it is not dominated by any other solution. The set of Pareto optimal solutions, called Pareto Front (PF), represents the general solution of the problem (3). Most methods for solving multi-objective optimisation problems, such as the Weighted Sum Method [43], convert them into simpler problems, in which a scalar function of the objectives is minimised or maximised. Under some assumptions, this gives a solution belonging to PF and is an acceptable compromise between all (possibly conflicting) objectives. However, the definition of "acceptable compromise" is left to the user, who must carefully define the objective weights a priori. On the contrary, in the context of Genetic Algorithms (see Section 2.2), it is possible to track the whole Pareto Front without deciding the weight to assign to each objective a priori and postponing instead the choice of a unique solution if needed by the user.

2.2. Genetic Algorithms

Genetic Algorithms [39] are a zero-order, population-based meta-heuristic method widely used to solve difficult optimisation problems. They mimic the optimum search as observed in nature, where living species evolve through recombination of their genetic pool. The algorithm starts with a population of randomly (or quasi-randomly) generated solutions, whose fitness function is evaluated. The *chromosome* of a solution (individual) is represented by the vector $\boldsymbol{p}$, while its fitness is the value $\omega(\boldsymbol{p})$. The individuals in a population are then ranked based on their fitness and an intermediate population is created by rearranging the previous one. High-fitness individuals may be duplicated, and poor-performing individuals may disappear. Individuals in the intermediate population are selected to mate, and, by recombination (*crossover*) of the parents' chromosomes, new individuals (*offspring*) are generated. These new individuals are the basis for the generation of a new population, which is evaluated after application of *mutation* with low probability (random changes in some genes, to increase exploration capability of the algorithm) and *elitism* (best individuals of the parent population may remain in the new population, to avoid losing promising solutions). The new population is in average better than the previous, and after evaluation it undergoes the same operators described, i.e. ranking, selection, crossover, mutation, elitism. The iterative process is stopped when some condition is met. In the problems described in this paper, the termination condition consisted of a fixed number of generations.

Thanks to population processing, multi-objective optimisation may be effectively handled by a GA without the need of defining a scalar measure of the objective vector $\boldsymbol{\omega} = [\omega_1,\ldots,\omega_N]^T$. The key concept of the Non-dominated Sorting Genetic Algorithm-II (NSGA-II, [44]) is that the evolution should be driven by two overall purposes: (a) search for the PF, and (b) avoiding premature convergence. This is achieved by slight modification of the operators described above. Objective (a) is obtained with ranking based on the non-domination concept instead of the fitness value. Premature convergence is avoided by adopting a selection algorithm based on crowding fitness, meaning that isolated solutions are preferred to solutions surrounded by many individuals. This approach represents the state-of-art in the field of multi-objective optimisation and is implemented in the software TOSCA [45], used in this work.

2.3. The numerical model

The numerical model utilised to simulate the cyclic response of a steel member is the smooth model proposed by Sivaselvan and Reinhorn [15]. This is a variation of the original Bouc-Wen model [10,11], and represents the cyclic behaviour of the plastic region at the end of a steel member as a zero-length element (plastic hinge) whose global response is determined by an ensemble of nonlinear springs (Fig. 1). Each spring represents a phenomenon observed in the cyclic response of structures. Even though the reference is to the couple moment-rotation (M-φ), this model applies to any work-conjugate pairs, according to the application under consideration. The model is implemented in the software Seismostruct [46].

Spring S1: Post-yielding hardening

This is a linear spring whose stiffness is equal to that of the hardening branch:

$$K_1 = k_{py} \cdot K_0 \tag{5}$$

where k_{py} is the post-yielding stiffness ratio and K_0 is the global elastic stiffness.

Spring S2: Hysteretic spring

Spring S2 is the spring governing the elastic-to-plastic transition and hysteretic behaviour. Its stiffness is equal to:

$$K_2 = (1-k_{py})K_0\left\{1-\left|\frac{M^*}{M_y^*}\right|^{N_{TRANS}}[\eta\ sgn(M^*\dot{\varphi})+(1-\eta)]\right\} \tag{6}$$

in which M^* is the portion of the applied moment shared by the hysteretic spring, $M_y^* = (1-k_{py})M_y$ with M_y yielding moment, N_{TRANS} is the power controlling the smoothness of the transition from elastic to inelastic range and η is a parameter controlling the shape of the unloading curve. Finally, $\dot{\varphi}$ is the rotation velocity.

Spring S3: Slip-lock spring

This spring governs pinching behaviour. Its stiffness is:

$$K_3 = \left\{\sqrt{\frac{2}{\pi}}\frac{R_S(\varphi_{max}^+ - \varphi_{max}^-)}{\sigma M_y^*}\exp\left[-\frac{1}{2}\left(\frac{M^*-\lambda M_y^*}{\sigma M_y^*}\right)^2\right]\right\}^{-1} \tag{7}$$

where R_S is a parameter controlling the slip length, φ_{max}^+ and φ_{max}^- are the maximum rotation reached on the positive and negative sides, respectively, σ is a measure of the moment range over which slip occurs, and λ the parameter controlling the slip at mean moment.

Spring 4: Gap-closing spring

This spring is responsible of the stiffness increment following a gap-closure. Its stiffness reads:

$$K_4 = \kappa K_0 N_{gap}(|\varphi| - \varphi_{gap})^{N_{gap}-1}U(|\varphi| - \varphi_{gap}) \tag{8}$$

where φ_{gap} is the gap-closing rotation, U is the Heaviside step function and κ and N_{gap} are spring parameters.

Stiffness and strength degradation

The model accounts for stiffness and strength degradation. The former is represented by a simplified formulation of the pivot rule [14], according to which the load-reversal branches are assumed to target a pivot point on the initial elastic branch at a distance αM_y on the opposite side. Stiffness degradation only occurs in the hysteretic spring S2.

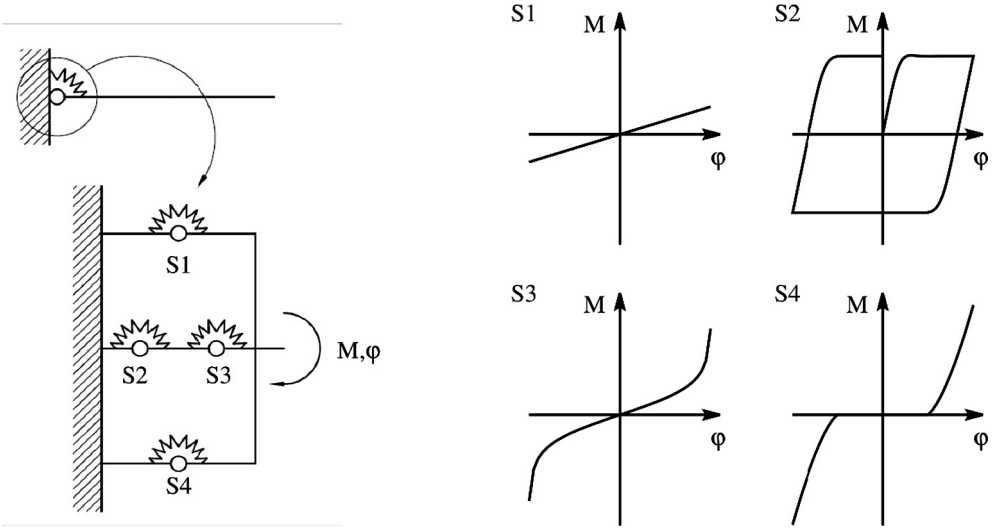

Fig. 1. The smooth model.

Strength degradation is modelled by reducing the capacity in the backbone curve according to the following rule:

$$M_y^{+/-} = M_{y0}^{+/-}\left[1-\left(\frac{\varphi_{max}^{+/-}}{\varphi_u^{+/-}}\right)^{\frac{1}{\beta_D}}\right]\left[1-\frac{\beta_E}{1-\beta_E}\frac{H}{H_{ult}}\right] \tag{9}$$

where $M_y^{+/-}$ is the positive or negative yield moment, $M_{y0}^{+/-}$ is the initial positive or negative yield moment, $\varphi_{max}^{+/-}$ is the maximum positive or negative rotation, $\varphi_u^{+/-}$ is the ultimate positive or negative rotation, H is the hysteretic energy dissipated and H_{ult} the hysteretic energy dissipated when loading monotonically to the ultimate rotation without any degradation. β_D and β_E are two degradation parameters.

3. The experimental programme

The calibration procedure described in Section 2 was applied onto the results of a series of experimental tests performed at the Laboratory of Materials and Structures of the Department of Civil Engineering of the University of Salerno. In particular, a monotonic and a cyclic test were carried out on a square hollow section member whose geometrical and material properties are reported in Table 1. These tests were originally designed to quantify and predict the flexural capacity of steel members [47]. In addition, a pseudo-dynamic test was performed in order to investigate the behaviour of the steel member under a generic loading history.

The experimental setups for the monotonic and the cyclic test were identical, and will be described in the following. Conversely,

Table 1
Geometrical (mm) and material (MPa) properties of the specimen.

Profile	Depth	Width	Thickness	Steel	Bolt diameter	Bolt class	Bolt number
250 × 250 × 8	250	250	8	S355	30	8.8	12

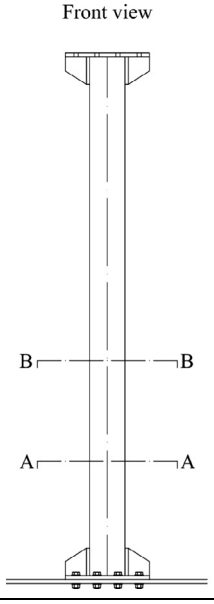

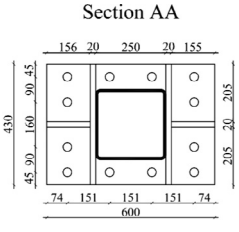

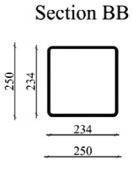

the details of the experimental equipment and configuration for the pseudo-dynamic test will be given in the relevant Section 3.3.

An MTS 243.35T hydraulic actuator with a maximum load capacity of 365 kN in compression and 240 kN in tension and a piston stroke equal to ±508 mm, fixed to a rigid steel braced frame acting as reaction wall, was used to apply the displacement history during the experimental tests. The column base was bolted to a rigid base and anchored to the laboratory strong floor by means of high strength dywidag bars. The actuator was also connected to a central unit controlling the displacements to apply to the specimen.

As the main scope of the tests was the investigation of the flexural behaviour of steel beams under monotonic and cyclic loads, the adopted scheme is the cantilever column, which reproduces the behaviour of a beam in a frame subjected to seismic actions. No axial load was applied on the column. The clear length L_n of experimental cantilever, i.e. the distance between the load application point and the column base, is equal to 1865 mm (Fig. 2).

3.1. Monotonic test

The loading history of the monotonic test is represented by a ramp under displacement control up to a value corresponding to a rotation equal to 0.21 rad. The displacement was applied with constant rate of 0.25 mm/s.

To evaluate the base plastic rotation, the displacement δ_c measured by the transducer of the actuator has been corrected by subtracting the elastic contribution due to the column flexural deformability, obtaining the corrected displacements δ_i:

$$\delta_i = \delta_c - \frac{F_i L_n^3}{3EI_c} \tag{10}$$

where F_i is the applied force, E is the Young modulus and I_c is the column second moment of area.

Consequently, starting from the measured forces F_i and the displacement δ_i, the moment versus plastic rotation curve $M_i - \varphi_i$ has been obtained as:

$$M_i = F_i \cdot L_n \text{ and } \varphi_i = \frac{\delta_i}{L_n} \tag{11}$$

Due to the occurrence of local buckling of the compressed flange, the moment-rotation curve exhibits a softening branch after the attainment of the maximum resistance (Fig. 3a). Each buckled flange, due to the compatibility of rotation at the corners of the cross-section, caused the deformation of the web (Fig. 3b). The maximum moment achieved during the experimental test was equal to 374.95 kN m.

3.2. Quasi-static cyclic test

The cyclic test was performed following the AISC loading protocol [25]. This procedure is characterised by the control of the interstorey drift angle, imposed on the test specimen as specified below (ϑ = chord rotation):

- 6 cycles with ϑ = 0.00375 rad;
- 6 cycles with ϑ = 0.005 rad;
- 6 cycles with ϑ = 0.0075 rad;
- 4 cycles with ϑ = 0.01 rad;
- 2 cycles with ϑ = 0.015 rad;
- 2 cycles with ϑ = 0.02 rad;
- 2 cycles with ϑ = 0.03 rad;
- 2 cycles with ϑ = 0.04 rad.

The displacements to apply to the loading application point are obtained from the chord rotations as $\delta = \vartheta \cdot L_n$. Like in the monotonic test, the applied velocity was equal to 0.25 mm/s.

In Fig. 4a, the moment-rotation plot of the cyclic test is shown, while the failure mechanism is displayed in Fig. 4b. The maximum moment recorded during the test is equal to 362 kN m. The cyclic experimental plot evidences that significant strength degradation arose due to both the cumulated energy dissipated during the loading history and the amplitude of the plastic rotation. In particular, the resistance reduction evidenced by the cyclic test compared to the monotonic test for the same value of rotation testifies the role played by the energy dissipation. These two different sources of strength degradation are explicitly taken into account by the numerical model in Eq. (9).

3.3. Pseudo-dynamic test

In order to apply a loading history corresponding to actual earthquake actions, the specimen was subjected to a pseudo-dynamic (PsD) test. By combining an on-line computer simulation of the dynamic problem (accounting for damping and inertial effects) with the experimental response providing the actual

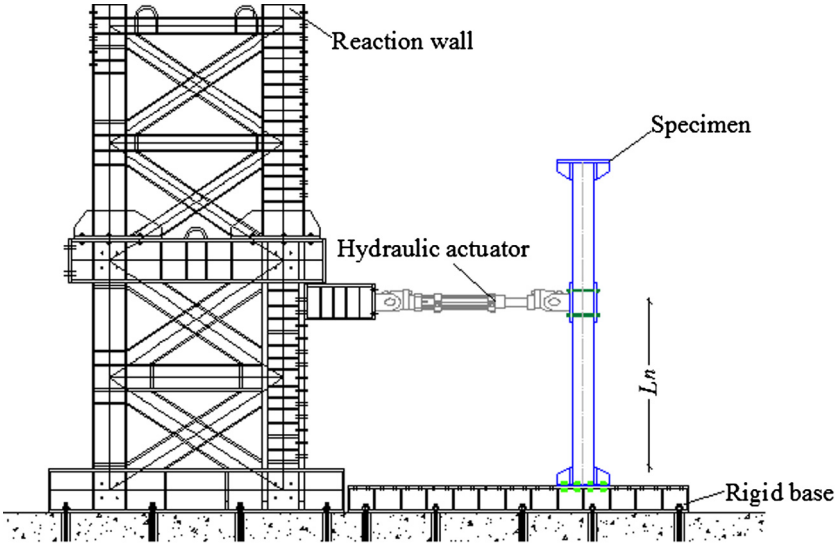

Fig. 2. Adopted set-up scheme for monotonic and cyclic tests.

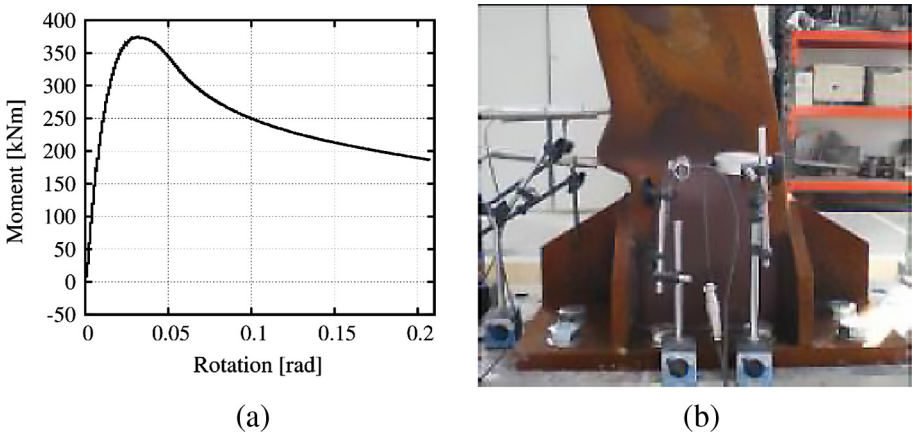

Fig. 3. Monotonic test: (a) moment vs. rotation plot, and (b) failure mechanism at the end of the test.

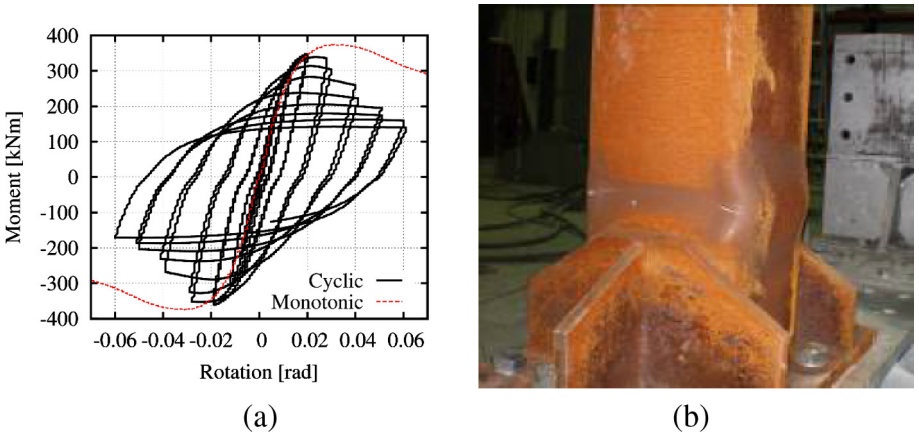

Fig. 4. Cyclic test: (a) moment vs. rotation plots, and (b) failure mechanism at the end of the cyclic test.

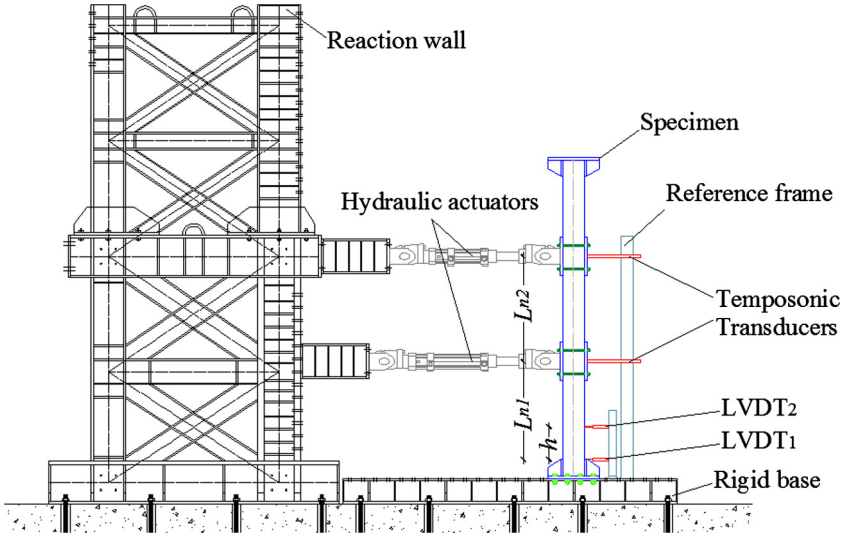

Fig. 5. Adopted set-up scheme for pseudo-dynamic tests.

restoring forces, this testing method provides realistic dynamic response histories even in case of nonlinear behaviour of severely damaged structures [48,49]. The structural system analysed by means of the pseudo-dynamic testing method is a two-degree-of-freedom system corresponding to the cantilever scheme depicted in Fig. 5. The diagonal mass matrix adopted for the pseudo-dynamic simulation is characterised by a mass value equal to 40 t. In particular, the first actuator (MTS 243.35T), with a maximum load capacity of 365 kN in compression and 240 kN in tension and a piston stroke equal to ±508 mm, was positioned at a

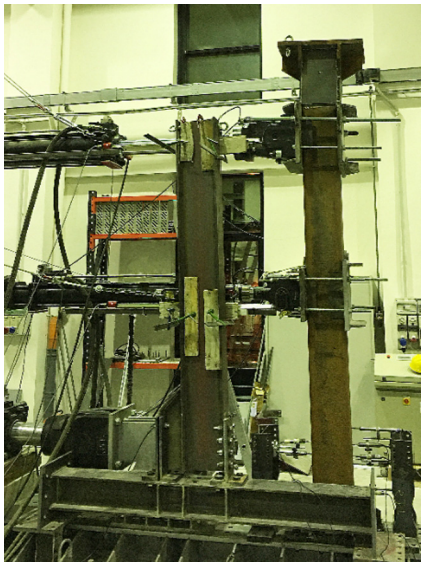

Fig. 6. View of the pseudo-dynamic test.

distance $L_{n.1}$ from the column end equal to 1250 mm, while the second actuator (MTS 243.45T), with a maximum load capacity of 650 kN in compression and 445 kN in tension and a piston stroke of ±533 mm, at a distance $L_{n.2}$ equal to 1140 mm. The actual displacements of the structure corresponding to the points where loads are applied, are measured by means of two external MTS Temposonic transducers (Figs. 5 and 6).

In addition, a set of two LVDTs was placed to evaluate the local rotation of the member at the base, one located at the end of the stiffened zone of the connection and one located at a distance of 400 mm from the previous one.

The test was carried out assuming no viscous damping and applying a loading velocity equal to 0.1 mm/s.

The pseudo-dynamic test was carried out with reference to Spitak (Armenia, 7 December 1988) earthquake record, as recorded at the station of Gukasyan (Armenia). This earthquake record (Magnitude 6.8 M_s, depth 5 km, duration 19.89 s) is essentially characterised by low amplitude cycles during the first ten seconds followed by few cycles with high amplitude and then a fast decay (Fig. 7).

In order to assure an earthquake intensity able to lead the specimen well in plastic range up to the occurrence of local buckling, Spitak earthquake record was scaled by means of a factor equal to 2.0 corresponding to a PGA equal to 0.398g.

In Fig. 8 the moment-rotation plot resulting from the pseudo-dynamic test is reported. In particular, starting from the forces

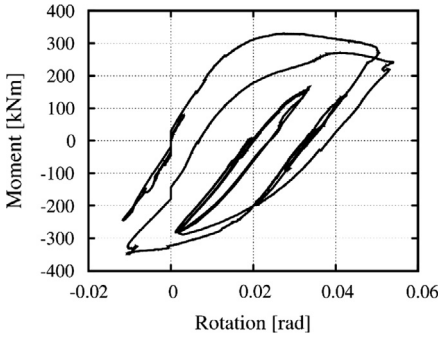

Fig. 8. Moment-rotation plot in the pseudo-dynamic test.

Fig. 9. Failure mechanism at the end of the pseudo-dynamic test.

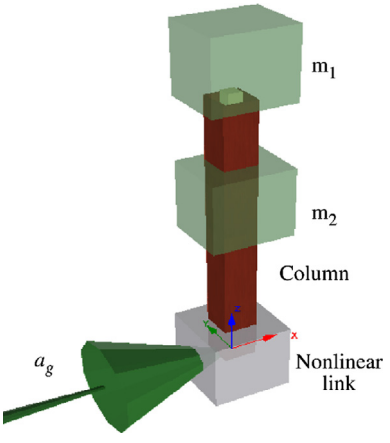

Fig. 10. FE model of the pseudo-dynamic test.

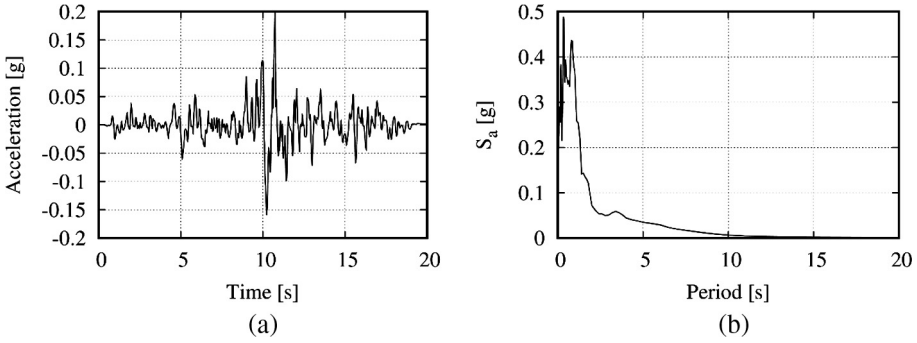

Fig. 7. (a) Spitak record and (b) 5%-damping response spectrum.

$F_{i.1}$ and $F_{i.2}$ measured by each actuator, the values of the moment M_i at the base of the cantilever has been obtained as:

$$M_i = F_{i.1} \cdot L_{n.1} + F_{i.2} \cdot L_{n.2} \tag{12}$$

The plastic rotation φ_i at the base of the cantilever has been determined as:

$$\varphi_i = \frac{\delta_{i.LVDT.2} - \delta_{i.LVDT.1}}{h} \tag{13}$$

where $\delta_{i.LVDT.1}$ and $\delta_{i.LVDT.2}$ are the displacements measured by means of the transducers and h is their distance as shown in Fig. 5.

The comparison between the behaviour of the member under monotonic test (Fig. 3), cyclic test (Fig. 4) and

Table 2
List of calibration analyses.

Label	Number of objectives	Quantity misfit (cyclic test)	Quantity misfit (monotone test)	Ultimate rotation φ_u (rad)
A1	1	Moment	–	0.21
A2	1	Moment	–	0.07
A3	1	Energy	–	0.21
A4	1	Energy	–	0.07
A5	2	Moment	Moment	0.21
A6	2	Energy	Moment	0.21

Table 3
Variation ranges for model parameters.

Parameters	Symbol	Minimum	Maximum	Step
Elastic stiffness (kN m)	K_0	25,000	40,000	100
Positive yielding moment (kN m)	M_y	351	500	1
Positive post-yielding stiffness ratio (–)	k_{py}	0.001	0.02	0.001
Stiffness degradation parameter (–)	α	2.0	20.0	0.1
Strength degradation parameter based on ductility (–)	β_D	0.001	3.0	0.001
Strength degradation parameter based on hysteretic energy (–)	β_E	0.001	1.0	0.001
Parameter controlling smoothness of elasto-plastic transition	$\log(N_{TRANS})$	−2	2	0.001
Parameter controlling the shape of unloading curve (–)	η	0.001	1.0	0.001
Parameter controlling the slip length (–)	R_S	0.0	2.0	0.01
Parameter controlling the slip curve (–)	σ	0.0	2.0	0.01
Parameter controlling the slip at mean moment (–)	λ	0.0	2.0	0.01

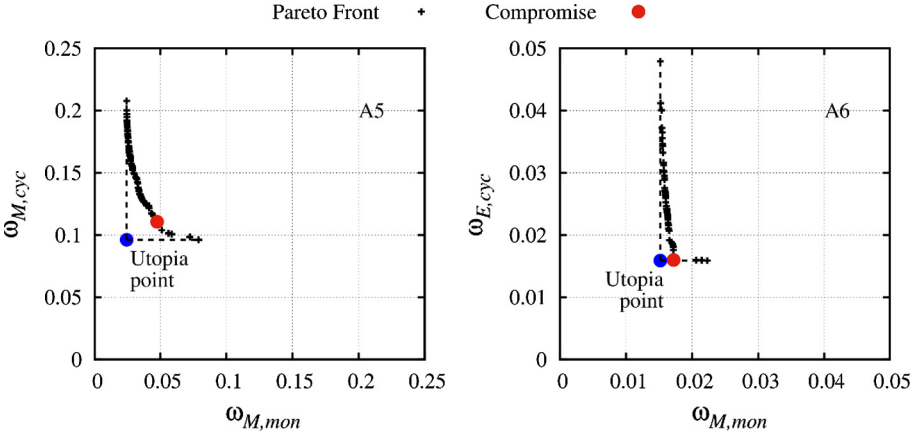

Fig. 11. Pareto fronts and compromise solutions for analyses A5 and A6.

Table 4
Optimal parameters for analyses A1–6.

Parameter		A1	A2	A3	A4	A5	A6	Monotonic
K_0	(kN m)	35,000	27,800	32,800	32,200	29,300	29,900	24,160
M_y	(kN m)	351	351	362	393	367	451	375
φ_u	(rad)	0.21	0.07	0.21	0.07	0.21	0.21	0.21
k_{py}	(–)	0.001	0.001	0.015	0.015	0.009	0.008	–
α	(–)	10.1	17.1	13.7	12.5	6.9	16.9	–
β_D	(–)	0.479	0.013	0.005	2.438	0.713	1.934	–
β_E	(–)	0.595	0.302	0.557	0.615	0.655	0.735	–
N_{TRANS}	(–)	2.30	2.21	9.10	2.31	3.27	1.71	–
η	(–)	0.517	0.702	0.823	0.576	0.603	0.84	–
R_S	(–)	0.7	0.61	0.65	0.58	0.54	0.85	–
σ	(–)	1.14	1.14	0.52	0.77	1.20	0.86	–
λ	(–)	1.59	1.52	1.18	1.59	1.64	1.68	–

pseudo-dynamic test (Fig. 8) highlights that for the examined ground motion, a softening response is exhibited as a consequence of local buckling (Fig. 9). This means that, in order to model such behaviour, the parameters of the analytical model need to be able to provide a cyclic envelope characterised by softening. However, such softening, also observed in the monotonic test, may not manifest during quasi-static cyclic tests, depending on the applied loading history.

4. Calibration results

4.1. Description of the analyses

The results of the previously described experimental programme were used to calibrate the parameters for the smooth model described in Section 2.3. To model the monotonic and cyclic tests, a FE model composed of a single link element was created, with one end point externally constrained and a rotation loading history applied to the other end. Conversely, the model of the pseudo-dynamic test consisted of two beam elements representing the column, and a link element connecting it to the ground. Two 40 t lumped masses were applied to the nodes corresponding to the load application points in the real test (Fig. 10). The Hilber-Hughes-Taylor integration scheme [50] with $\alpha = -0.1$, $\beta = 0.3025$ and $\gamma = 0.6$ was employed.

Different analyses were performed. They differ for the quantity whose misfit was minimised, the assumption about the ultimate rotation and the number of objectives. Two quantities have been considered: the bending moment $M(t)$ and the energy history $E(t)$. Here the parameter t may be the real time or an ordering parameter (pseudo-time) for quasi-static analyses. Energy history is defined starting from the moment and rotation histories, $M(t)$ and $\varphi(t)$ respectively, as:

$$E(t) = \int_0^{\varphi(t)} M(\varphi(t))d\varphi = \int_0^t M(\tau)\frac{d\varphi}{d\tau}d\tau \tag{14}$$

Therefore, depending on the considered quantity, the vectors $\boldsymbol{y_{exp}}$ and $\boldsymbol{y_c}$ in Eq. (2) collect $M_i = M(t_i)$ (resp. $E_i = E(t_i)$) at instants t_i. The cost functions (2) thus becomes:

$$\omega_M(\boldsymbol{p}) = \frac{\sqrt{\sum_{i=1}^{T}(M_{exp,i} - M_{c,i}(\boldsymbol{p}))^2}}{\sqrt{\sum_{i=1}^{T}M_{exp,i}^2}} \tag{15}$$

when moment misfit is minimised, and:

$$\omega_E(\boldsymbol{p}) = \frac{\sqrt{\sum_{i=1}^{T}(E_{exp,i} - E_{c,i}(\boldsymbol{p}))^2}}{\sqrt{\sum_{i=1}^{T}E_{exp,i}^2}} \tag{16}$$

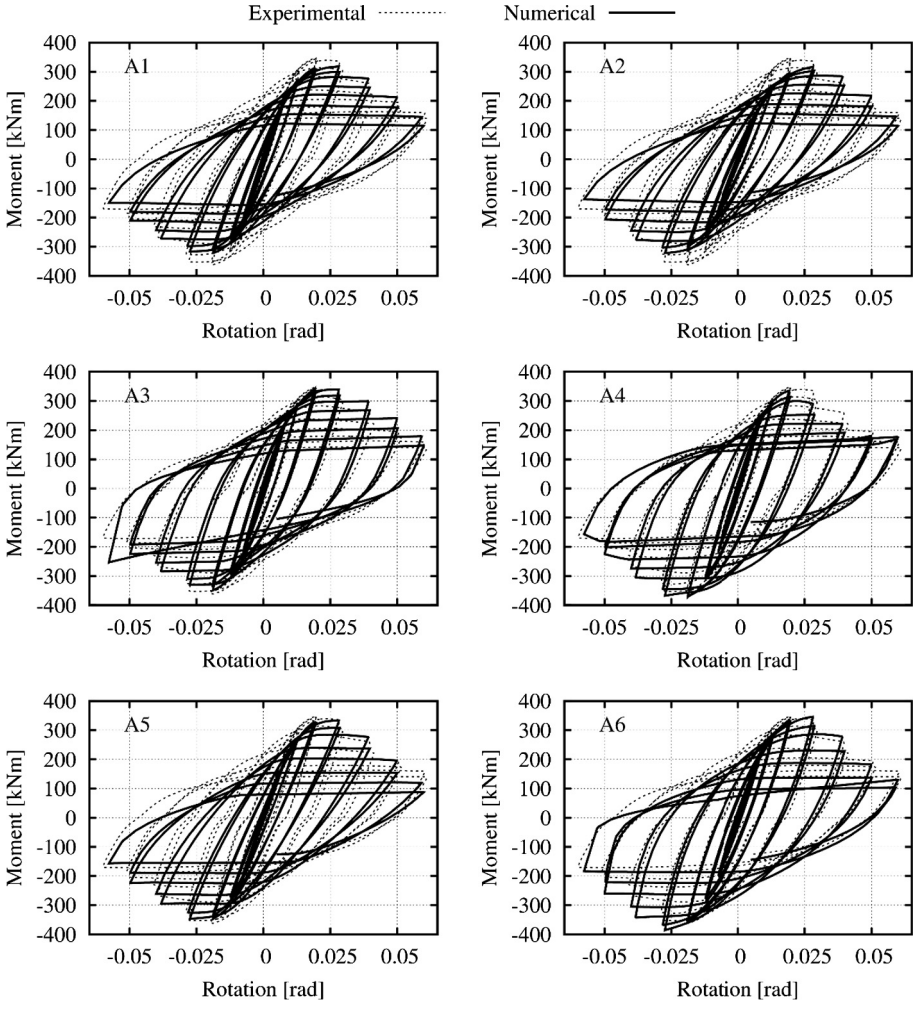

Fig. 12. Cyclic moment-rotation plots for analyses A1–6.

when energy misfit is minimised. The subscripts *exp* and *c* refer to the experimental and computed quantities respectively and T is the last time step. Because the AISC protocol is characterised by a large number of cycles in the elastic branch, the summation in (15) could include a large number of terms with small error which may represent a considerable part of the overall misfit ω_M. For this reason, in order to discard the initial elastic cycles, the misfit ω_M was evaluated considering those cycles where the energy $E(t)$ was greater than 20% the final experimental energy $E_{exp,T}$.

The analyses carried out to identify the criteria leading to the best calibration of the numerical model are summarised in Table 2. Analyses A1 and A2 reproduce mathematically what is usually done when the parameters matching the experimental and numerical moment-rotation plots are searched for. These two analyses only differ in the assumption about the ultimate rotation. In particular, analysis A1 is carried out by assuming for the ultimate rotation of the numerical model the one obtained from the monotonic test. Conversely, in analysis A2 such parameter of the numerical model has been assumed equal to 0.07 rad, i.e. the ultimate rotation occurred during the cyclic test. The same difference was considered for analyses A3 and A4, where energy misfit was minimised. Analyses A5 and A6 are characterised by the adoption of two objectives to minimise, each referring to one of the available experimental tests, i.e. the cyclic and the monotonic test. Analysis A5 accounts for moment misfit in both tests, while analysis A6 accounts for energy misfit occurring in the modelling of the cyclic test and for moment misfit in the modelling of the monotonic test. The variation ranges for the parameters $\boldsymbol{p}$ entering the model are reported in Table 3. The positive ultimate rotation φ_u was assumed equal to 0.21 or 0.07 according to the analysis hypothesis (see Table 2). The negative quantities corresponding to M_y, φ_u, k_{py} were assumed to be opposite to their positive counterparts (symmetric behaviour). The total number of variable parameters is thus equal to 11.

Even though pinching is not visible from the experimental plots (see Figs. 4 and 8), parameters R_S, σ, λ were assumed as unknown, because the slip-locking spring S3 modelling pinching works in series with the hysteretic spring S2 (Fig. 1) and thus an arbitrary choice for the values of these parameters unavoidably affects the identification of parameters K_0, M_y, k_{py}, N_{TRANS}. Conversely, assuming a large value for gap-closing rotation φ_{gap} disables gap-closing spring S4 working in parallel with the other springs. Since gap-closing effects, i.e. stiffening at high deformation, were not encountered in the cyclic response, it is possible to discard its parameters in the optimisation procedure.

The GA parameters for the optimisation analyses are the following:

- Population: 50 individuals;
- Initial population generated by the Sobol algorithm [51];
- Number of generations: 100;

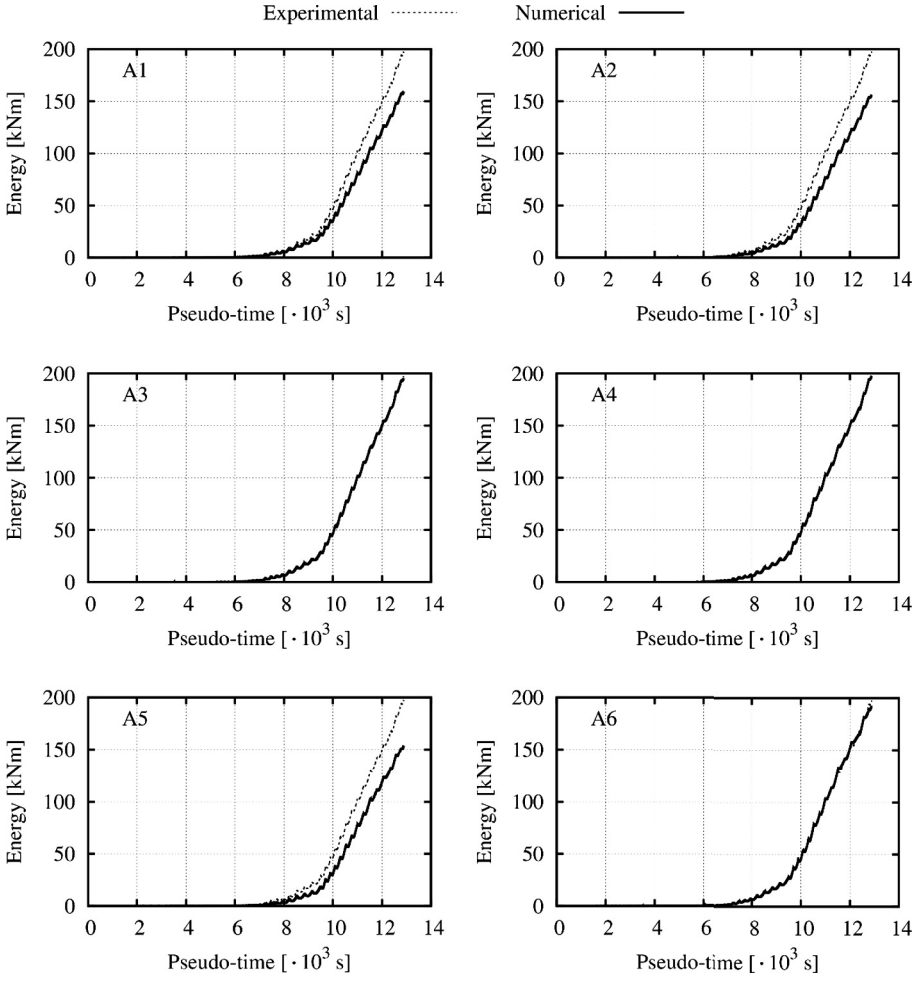

Fig. 13. Cyclic energy-pseudotime plots for analyses A1–A6.

- Selection: Stochastic Universal Sampling [52], with linear ranking based on domination and scaling pressure equal to 2.0;
- Crossover: Blend-α [53], with α = 2.0;
- Crossover probability: 1.0;
- Mutation probability: 0.007.

These values were assumed based on previous research [45], as they allow for a correct balance between the conflicting needs of exploration and exploitation which are typical of nonlinear optimisation.

When comparing analyses A1–6 it is necessary to define the "solution" of the calibration problem. While this is obvious for analyses A1–4 in which a single objective is to be minimised, for analyses A5–6 the general solution is, as stated above, the Pareto Front, i.e. an ensemble of possible solutions. In Fig. 11, the PFs obtained in analyses A5–6 are shown (with the subscripts *mon* and *cyc* referring to the monotonic and cyclic test, respectively), and the compromise solutions chosen for the comparisons described in next sub-sections are highlighted. Following general concepts of L-curves in ill-posed inverse problems [54], a fair balance between the two objectives is represented by the "corner" point in the L-shaped PF. In mathematical terms, this point is the element of the PF having shortest distance from the "utopia point" defined as the theoretical point which would minimise both objectives at the same time. It is important to underline again that even though a unique solution is finally chosen, unlike the Weighted Sum Method no prior definition is needed to weight the two objectives properly.

The results of the six analyses in terms of parameter values are displayed in Table 4, along with the values estimated from the monotonic test. For these latter values, except for the initial stiffness and the ultimate rotation, there is always a certain degree of subjectivity in the definition of M_y. As the monotonic test result is characterised by a softening branch due to local buckling, the value reported in last column of Table 4 is equal to the maximum moment. This subjectivity would be even greater if one wished to estimate this parameter from a cyclic test only (for instance considering the envelope), because in that case even the maximum moment would depend on the loading history. For this reason, in the calibration procedure developed in this work, no prior information was considered for any parameter, and all of them were calibrated simultaneously.

4.2. Quasi-static cyclic test

The moment-rotation plots for the best individuals obtained in analyses A1–6 are shown in Fig. 12 and compared with the experimental data.

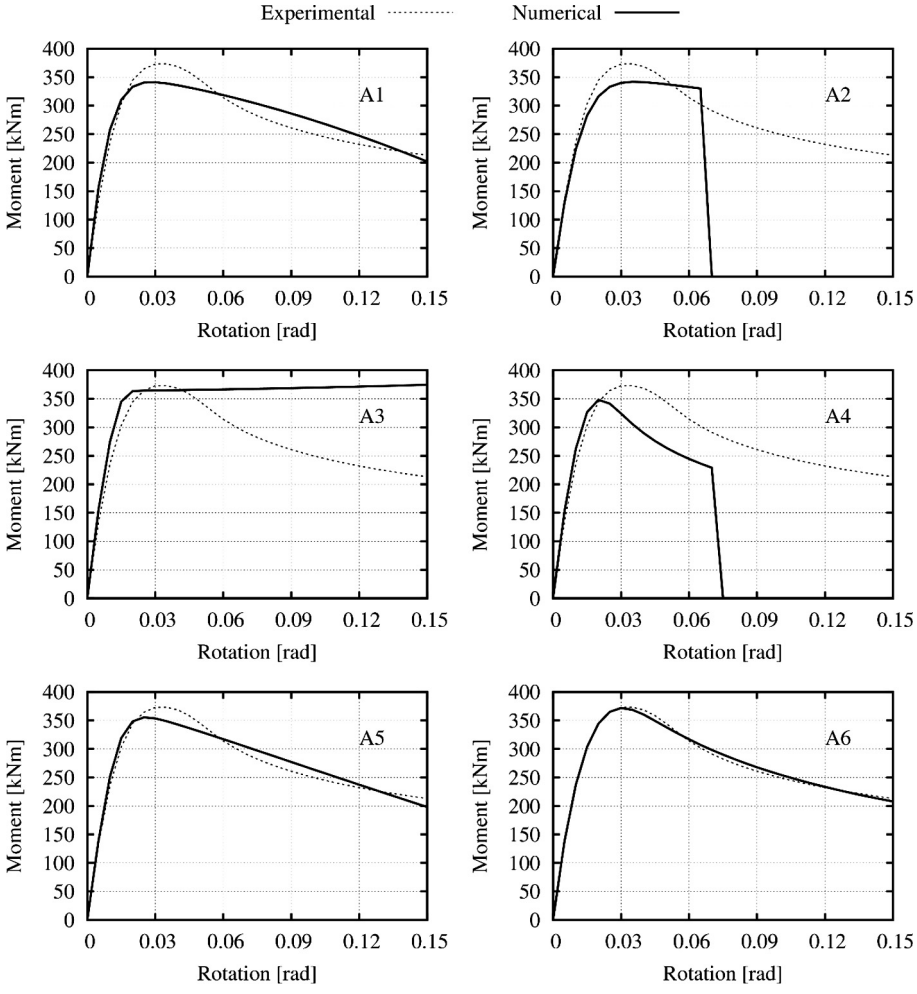

Fig. 14. Monotonic moment-rotation plots for analyses A1–6.

Analyses A1–2 seem to slightly underestimate the maximum moment. Analyses A3 and A6, on the contrary, seem not to match the experimental data in the last cycles. This is a natural consequence of the objective function: energy values depend on the previous history, meaning that last numerical M-φ loops may be considerably different from the experimental records without significantly affecting the overall energy misfit.

In general, however, no model clearly outperforms the others if one only looks at the M-φ plots. The matter is different if E-t plots are compared (Fig. 13). All the analyses where the cost function is based on moment (A1, A2, A5) underestimate the dissipated energy by almost 25%; on the contrary, analyses A3, A4, A6, where energy is explicitly taken into account in the calibration, show a very good match. It can thus be argued, that, at least for the studied case, while minimising energy misfit (analyses A3, A4 and A6) seems to imply a good M-φ match, the contrary does not hold, and minimising moment misfit may entail a considerable energy error.

4.3. Monotonic test

The monotonic test is used as calibration test in analyses A5 and A6 only. It thus represents a validation test for the other analyses. The comparison between experimental and numerical results is displayed in Fig. 14.

The advantages of an approach accounting for data from monotonic test are clearly visible. A good match in M-φ plot for the cyclic test (analyses A1–4) is by no means representative of the monotonic behaviour of the steel member. The strength degradation observed in the cyclic test may be modelled by both ductility- or energy-based contributions in the smooth model (Eq. (9)), and without any information coming from a monotonic test, an automatic optimisation procedure cannot distinguish between them. This is particularly evident if one looks at the results of analyses A1 and A3: similar strength degradation in the cyclic test (Fig. 12) may be attained by parameters leading to either a degrading or a hardening model when monotonic behaviour is modelled (Fig. 14).

Furthermore, the ultimate rotation observed in the cyclic test (and prescribed by the standard AISC) cannot be considered as ultimate rotation *tout-court*, physical characteristic of the connection, since it may or may not be exceeded depending on the loading history. Erroneous definition of the ultimate rotation may lead to gross errors in the monotonic test prediction (Fig. 14, analyses A2 and A4), and in any loading history where the limit prescribed by the protocol may be overcome.

4.4. Pseudo-dynamic test

The comparison between experimental and numerical responses are displayed in Figs. 15–18, as M-φ plots as well as displacements at the first and second mass and energy versus time. Since Spitak record is characterised by a number of small cycles

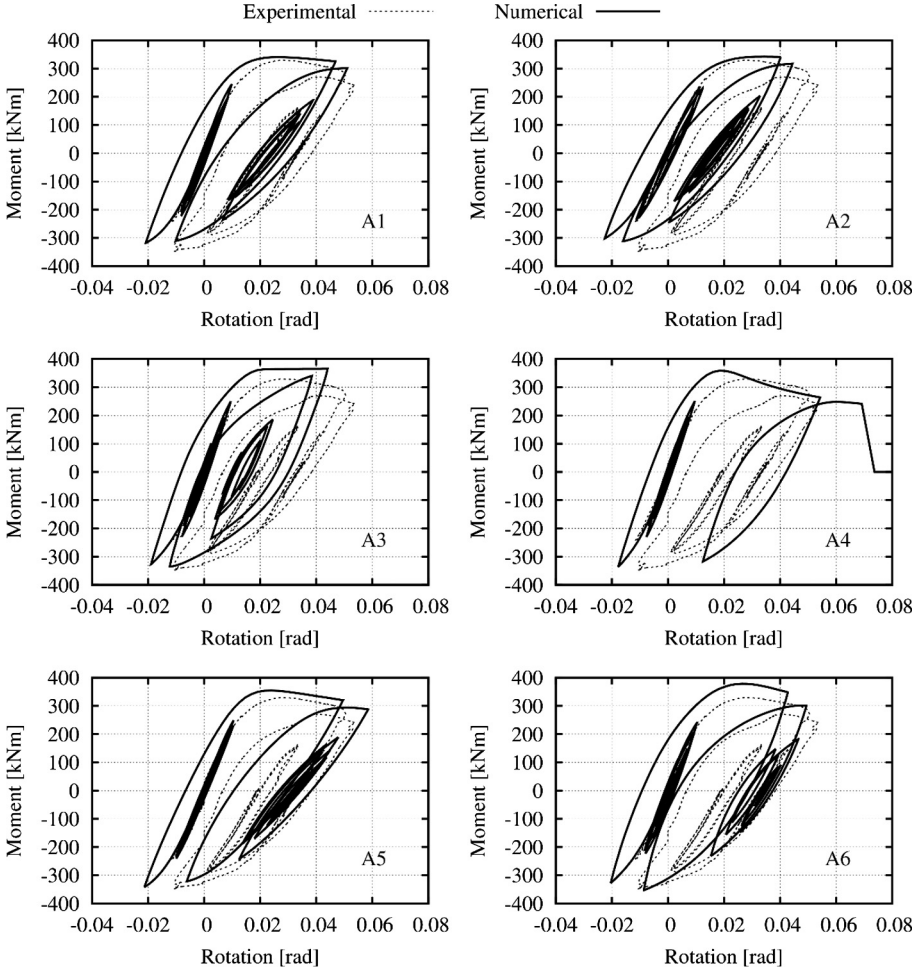

Fig. 15. Pseudo-dynamic moment-rotation plots for analyses A1–6.

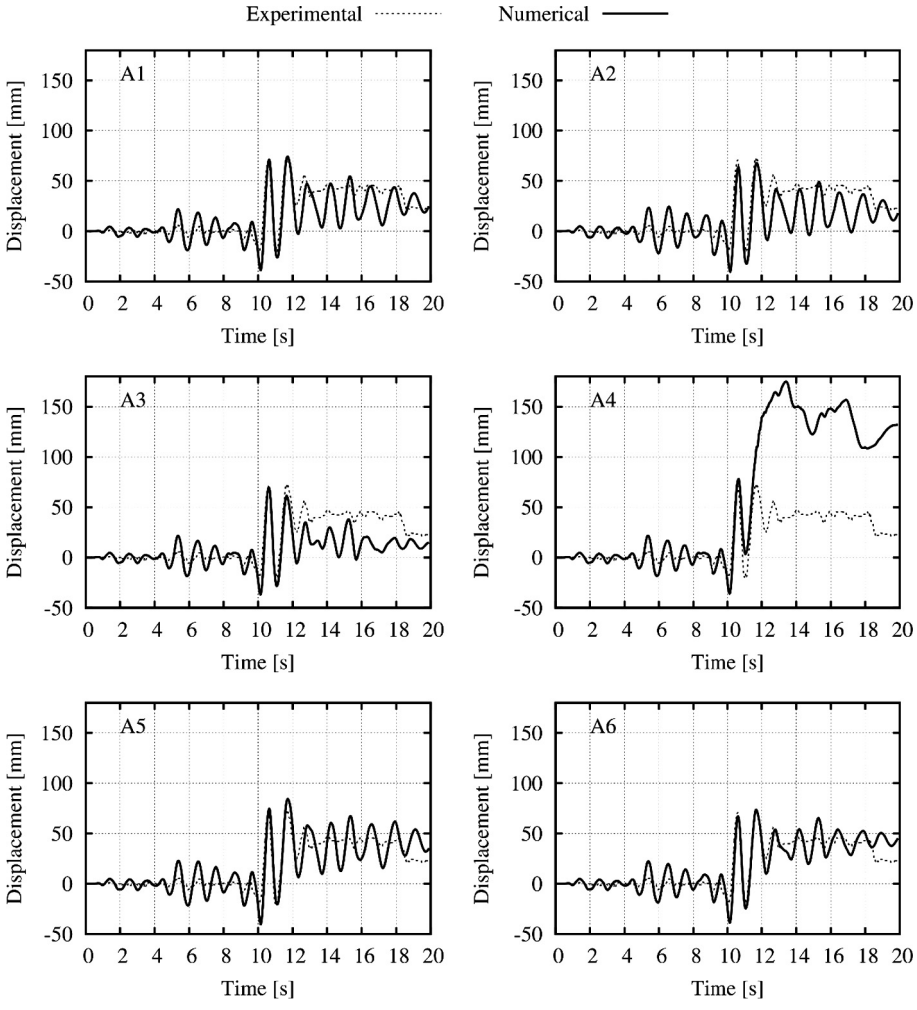

Fig. 16. Pseudo-dynamic experimental and numerical displacement at the first mass for analyses A1–6.

followed by two strong impulses, the response of the specimen under monotonic loading is expected to play an important role. This is confirmed by all the responses, which are best matched by the optimum models of analyses A5 and A6. In particular, the rotation demand is underestimated by analyses A2 and A3, and overestimated by analysis A4, while analyses A1, A5 and A6 predict the maximum rotation with reasonable accuracy. This reflects on the displacements at the first and second masses (Figs. 16 and 17): while the maximum is captured by almost all the models (with the exception of analysis A4, which strongly overestimates it), the postpeak response (residual deformation) is matched well only by analyses A5–A6. This may be important in case of incremental dynamic analyses. The energy is approximately matched by all solutions.

5. Discussion and conclusions

In this work, some strategies for calibrating cyclic models for steel members are critically discussed with reference to a recently completed experimental programme carried out at the University of Salerno. The final aim of this investigation was assessing if the calibration of a phenomenological numerical model accounting for stiffness and strength degradation based on the result of a cyclic test may accurately predict the response under different conditions. A secondary objective was to set up an automatic calibration procedure for cyclic models of members where the hysteretic behaviour is governed by yielding and possibly local buckling.

Three different experimental tests were carried out on a steel square hollow member: (i) a monotonic flexural test, (ii) a quasi-static cyclic test, and (iii) a pseudo-dynamic test with Spitak ground-motion record with scale factor equal to 2 applied at the column base. In the pseudo-dynamic test, two fictitious 40 t masses at 1250 mm and 2392 mm, respectively, were considered.

The calibration was performed minimising the response misfit between experimental test and numerical simulation. Six cases were considered, differing in the quantity misfit to minimise (moment or energy), the assumption about the ultimate rotation, and accounting or not for the monotonic test data.

Whereas in principle the equality of moment history between experimental and numerical test implies equality of energy, inevitable measurement and model errors make the minimum misfit to be different from zero. This suggests that moment and energy cost function minima may be attained by possibly different models. The results show that a calibration of a cyclic response based on the moment misfit can significantly underestimate energy dissipation. On the contrary, in the case studied in this work, the opposite does not seem to happen and the energy-optimal model is satisfactorily accurate in predicting

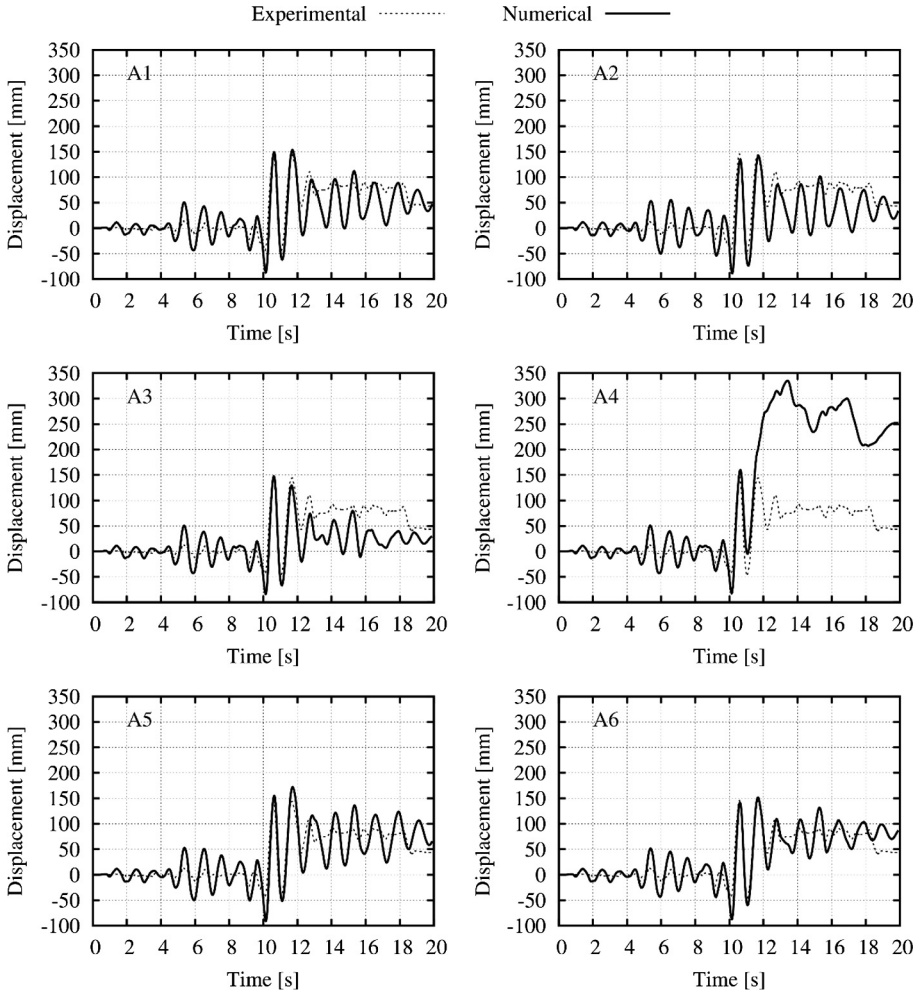

Fig. 17. Pseudo-dynamic experimental and numerical displacement at the second mass for analyses A1–6.

M-φ history. So, it is suggested to perform the calibration of the model under a quasi-static cyclic test by fitting energy rather than the moment history.

A second most important result regards the predictive capability of a model calibrated on the cyclic test only. It is apparent from the results of this analysis that two models fitting equally well the cyclic response may show significantly different monotonic responses. Furthermore, the ultimate rotation required by the formulation of the smooth model cannot be assumed equal to that observed in the cyclic test because it is not a fixed characteristic of the member, as it depends on the history loading. The ultimate rotation of the monotonic test should be used instead, as pointed out in [32] with reference to Ibarra-Medina-Krawinkler hysteretic model [16]. The ill-posedness of the inverse problem is confirmed by the validation against the results of the pseudo-dynamic test. The optimum model of analysis A4, which fits the experimental response of the cyclic test remarkably well, failed in predicting the response of the structure under Spitak ground motion.

Whereas a different loading protocol could overcome these drawbacks, in this work it is observed that including the information gathered by a monotonic test into the procedure by performing the calibration by means of multi-objective optimisation may give satisfactory results. The recommendation of considering the monotonic response along with the cyclic one was already pointed out in [17,18,55], even though in these works no multi-objective approach was considered. The accuracy of the proposed calibration is evident by comparing the responses of the calibrated models under Spitak ground-motion with the results of the pseudo-dynamic test. Unlike the others, the models calibrated by applying the proposed procedure accurately predict dissipated energy, M-φ history and both maximum and residual displacement.

It is important to note that even though one earthquake was considered as validation in the pseudo-dynamic test, it has some attributes which highlight the lack of robustness of a calibration performed by means of a cyclic test only. In fact, Spitak record is characterised by several small-amplitude cycles followed by few large-amplitude cycles. Excursion into plastic branch thus occurs before any degradation of mechanical properties, and for this reason the monotonic behaviour plays a crucial role. Under different earthquakes, this feature may be more or less pronounced.

Based on the results described, automatic calibration as proposed in this work seems to be promising. However, further research is needed to validate or improve the strategy (for example considering the addition of more tests or objectives). Furthermore, the ill-posedness of the inverse problem of estimating model parameters from the test may be alleviated by fixing some of them a priori if it is known that their importance in the response is low. This involves a careful analysis of the sensitivity of the response on the parameters under different loading conditions, left here for future research.

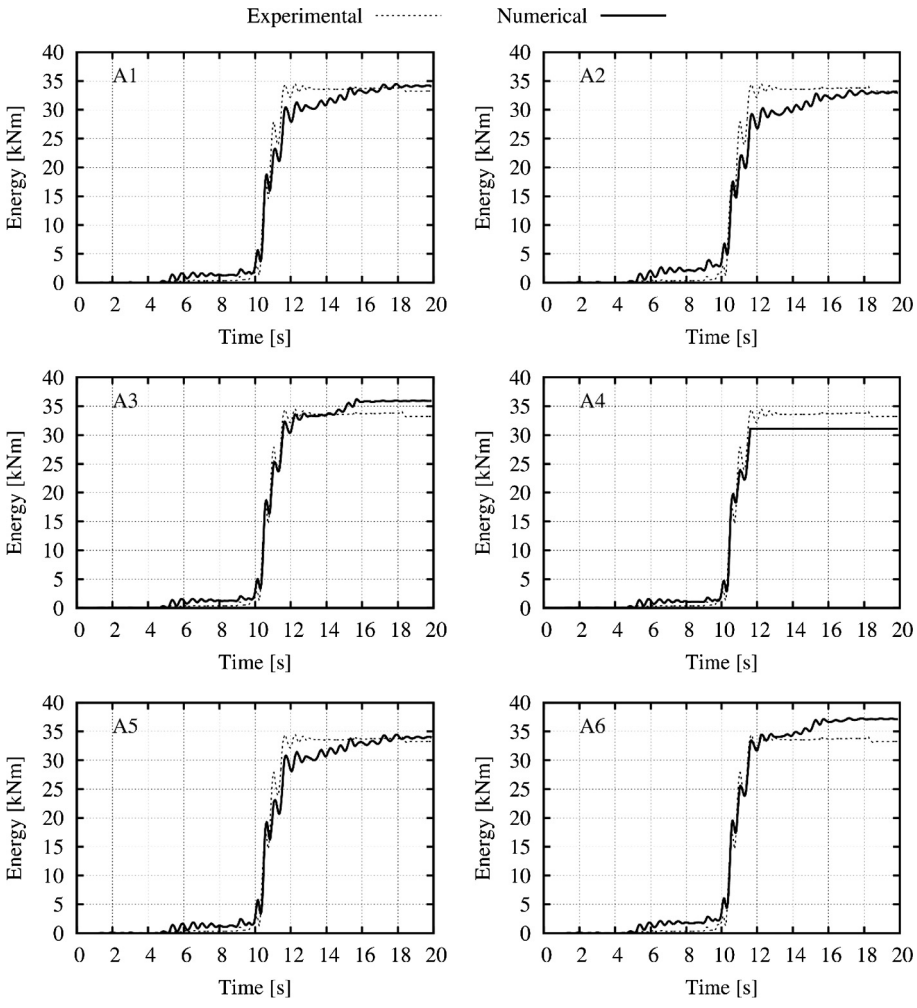

Fig. 18. Pseudo-dynamic experimental and numerical energy-time plots for analyses A1–6.

Acknowledgements

The first author received financial support from research project FERGE, identification number: 300395PON14GALDI.

References

[1] Haddad M. Concentric tubular steel braces subjected to seismic loading: finite element modeling. J Constr Steel Res 2015;104:155–66.

[2] Moradi S, Alam M. Finite-element simulation of posttensioned steel connections with bolted angles under cyclic loading. ASCE J Struct Eng 2016;142(1).

[3] Latour M, Rizzano G. Cyclic behavior and modeling of a dissipative connector for cross-laminated timber panel buildings. J Earthquake Eng 2015;19 (1):137–71.

[4] Nastri E, Montuori R, Piluso V. Seismic design of MRF-EBF dual systems with vertical links: EC8 vs plastic design. J Earthquake Eng 2015;19(3):480–504.

[5] Montuori R, Muscati R. A general design procedure for failure mechanism control of reinforced concrete frames. Eng Struct 2016;118:137–55.

[6] Latour M, Piluso V, Rizzano G. Rotational behaviour of column base plate connections: experimental analysis and modelling. Eng Struct 2014;68:14–23.

[7] Latour M, Rizzano G. A theoretical model for predicting the rotational capacity of steel base joints. J Constr Steel Res 2013;91:89–99.

[8] Latour M, Rizzano G. Full strength design of column base connections accounting for random material variability. Eng Struct 2013;48:458–71.

[9] Takeda T, Sozen M, Nielsen N. Reinforced concrete response to simulated earthquakes. J Struct Div 1970;96(12):2557–73.

[10] Bouc R. Forced vibration of mechanical systems with hysteresis. In: Proceedings of the fourth conference on non-linear oscillation, Prague, Czechoslovakia.

[11] Wen Y-K. Method for random vibration of hysteretic systems. ASCE J Eng Mech Div 1976;102(2):249–63.

[12] Ramberg W, Osgood W. Description of stress–strain curves by three parameters. Technical note 902. National Advisory Committee on Aeronautics; 1943.

[13] Richard RM, Abbott BJ. Versatile elasto-plastic stress-strain formula. J Eng Mech Div 1975;101(4):511–5.

[14] Dowell RK, Seible F, Wilson EL. Pivot hysteresis model for reinforced concrete members. ACI Struct J 1998;95(5):607–17.

[15] Sivaselvan MV, Reinhorn AM. Hysteretic models for deteriorating inelastic structures. J Eng Mech 2000;126(6):633–40.

[16] Ibarra LF, Medina RA, Krawinkler H. Hysteretic models that incorporate strength and stiffness deterioration. Earthquake Eng Struct Dynam 2005;34:1489–511.

[17] Lignos D, Krawinkler H, Whittaker A. Prediction and validation of sidesway collapse of two scale models of a 4-story steel moment frame. Earthquake Eng Struct Dynam 2011;40(7):807–25.

[18] Lignos D, Krawinkler H. Development and utilization of structural component databases for performance-based earthquake engineering. J Struct Eng (United States) 2013;139(8):1382–94.

[19] Skalomenos KA, Hatzigeorgiou GD, Beskos DE. Parameter identification of three hysteretic models for the simulation of the response of CFT columns to cyclic loading. Eng Struct 2014;61:44–60.

[20] Porter M. Sequential phased displacement (SPD) procedure for TCCMAR testing. In: 3rd Meeting of the joint technical coordinating committee on masonry research, US-Japan coordinated program, Tomamu, Japan.

[21] ISO 16670:2003. Timber structures – joints made with mechanical fasteners – quasi-static reversed-cyclic test method. International Organization for Standardization (ISO); 2003.

[22] Krawinkler H, Parisi F, Ibarra L, Ayoub A, Medina R. Development of a testing protocol for woodframe structures. CUREE, publication no. W-02; 2001.

[23] EN 15129:2010. Anti-seismic devices. European Committee for Standardization (CEN); 2010.

[24] ECCS. Recommended testing procedure for assessing the behaviour of structural steel elements under cyclic loads. European Convention for Constructional Steelwork – Technical Committee 1 – Structural Safety and Loadings – Technical Working Group 1.3 – Seismic Design; 1986.

[25] American Institute of Steel Construction. ANSI/AISC 341-10. AISC; 2010.
[26] Richards P, Uang C. Testing protocol for short links in eccentrically braced frames. J Struct Eng 2006;132(8):1183–91.
[27] Ramadan T, Ghobarah A. Analytical model for shear-link behavior. J Struct Eng (United States) 1995;121(11):1574–80.
[28] Mergos PE, Beyer K. Loading protocols for European regions of low to moderate seismicity. Bull Earthquake Eng 2014;12:2507–30.
[29] Stewart W. The seismic design of plywood sheathed shear walls PhD thesis. New Zealand: University of Canterbury; 1987.
[30] Krawinkler H, Gupta A, Medina R, Luco N. Development of loading histories for testing of steel beam-to-column assemblies. SAC background report SAC/BD-00/10; 2000.
[31] Gatto K, Uang C-M. Effects of loading protocol on the cyclic response of woodframe shearwalls. J Struct Eng 2003;129(10):1384–93.
[32] Lignos DG, Krawinkler H. Deterioration modeling of steel components in support of collapse prediction of steel moment frames under earthquake loading. J Struct Eng 2011;137(11):1291–302.
[33] Nogueiro P, Silva LSd, Bento R, Simões R. Numerical implementation and calibration of a hysteretic model with pinching for the cyclic response of steel joints. Adv Steel Constr 2007;3(1):459–84.
[34] Chisari C, Macorini L, Amadio C, Izzuddin BA. An inverse analysis procedure for material parameter identification of mortar joints in unreinforced masonry. Comput Struct 2015;155:97–105.
[35] Chisari C, Bedon C, Amadio C. Dynamic and static identification of base-isolated bridges using Genetic Algorithms. Eng Struct 2015;102:80–92.
[36] Byrd RH, Schnabel RB, Shultz GA. A trust region algorithm for nonlinearly constrained optimization. SIAM J Numer Anal 1987;24(5):1152–70.
[37] Boggs PT, Tolle JW. Sequential quadratic programming. Acta Numer 1995;4:1–51.
[38] Nelder J, Mead R. A simplex method for function minimization. Comput J 1965;7(4):308–13.
[39] Goldberg DE. Genetic Algorithms in search, optimization and machine learning. Addison-Wesley; 1989.
[40] The American Society For Mechanical Engineers. Guide for verification and validation in computational solid mechanics. ASME; 2006.
[41] Trucano T, Swiler L, Igusa T, Oberkampf W, Pilch M. Calibration, validation, and sensitivity analysis: what's what. Reliab Eng Syst Saf 2006;91:1331–57.
[42] Miettinen K. Nonlinear multiobjective optimization. Springer; 1999.
[43] Stadler W. A survey of multicriteria optimization, or the vector maximum problem. J Optim Theory Appl 1979;29:1–52.
[44] Deb K, Pratap A, Agarwal S, Meyarivan T. A fast and elitist multiobjective Genetic Algorithm: NSGA-II. IEEE Trans Evol Comput 2002;6(2):182–97.
[45] Chisari C. Inverse techniques for model identification of masonry structures PhD thesis. University of Trieste; 2015.
[46] Seismosoft. SeismoStruct v7.0 – a computer program for static and dynamic nonlinear analysis of framed structures; 2014 [Online]. Available: <http://www.seismosoft.com> [accessed 13 April 2016].
[47] D'Aniello M, Landolfo R, Piluso V, Rizzano G. Ultimate behavior of steel beams under non-uniform bending. J Constr Steel Res 2012;78:144–58.
[48] Shing P, Mahin S. Pseudodynamic test method for seismic performance evaluation: theory and implementation. Berkeley: Earthquake Engineering Research Center UCB/EERC-8'1/01; University of California; 1984.
[49] Shing PB, Nakashima M, Bursi O. Application of pseudodynamic test method to structural research. Earthquake Spectra 1996;12(1):29–56.
[50] Hilber HM, Hughes T, Taylor R. Improved numerical dissipation for time integration algorithms in structural dynamics. Earthquake Eng Struct Dynam 1977;5(3):283–92.
[51] Antonov IA, Saleev VM. An economic method of computing LP tau-sequence. USSR Comput Math Math Phys 1979;19(1):252–6.
[52] Baker JE. Reducing bias and inefficiency in the selection algorithm. In: Second international conference on Genetic Algorithms and their application, Hillsdale, New Jersey.
[53] Eshelman LJ, Schaffer JD. Real-coded Genetic Algorithms and interval schemata. In: Foundations of Genetic Algorithms, San Mateo, Morgan-Kaufman. p. 187–202.
[54] Hansen PC, O'Leary DP. The use of the L-curve in the regularization of discrete Ill-posed problems. SIAM J Sci Comput 1993;14(6):1487–503.
[55] Krawinkler H. Loading histories for cyclic tests in support of performance assessment of structural components. In: The 3rd international conference on advances in experimental structural engineering, San Francisco.